Supplementary Information

Midgap-state-mediated two-steps photoexcitation in nitrogen defective g-C$_3$N$_4$ atomic layers for superior photocatalytic CO$_2$ reduction

Jie-Yinn Tang[a], Xin Ying Kong[a], Boon-Junn Ng[a], Yi-Hao Chew[a], Abdul Rahman Mohamed[b] and Siang-Piao Chai*[a]

[a]Multidisciplinary Platform of Advanced Engineering, Chemical Engineering Discipline, School of Engineering, Monash University, Jalan Lagoon Selatan, Bandar Sunway, 47500 Selangor, Malaysia.

[b]Low Carbon Economy (LCE) Group, School of Chemical Engineering, Universiti Sains Malaysia, Engineering Campus, Seri Ampangan, 14300 Nibong Tebal, Pulau Pinang, Malaysia.

*Correspondence to: chai.siang.piao@monash.edu

S1 Experimental procedure for bulk g-C$_3$N$_4$ nanosheets

Bulk g-C$_3$N$_4$ nanosheets (CN-B) were synthesized via thermal polymerization route with melamine as the precursor. 2g of melamine powder was transferred into a 50 ml alumina crucible with closed lid. The crucible was placed in a muffle furnace and heated at a designated temperature of 550°C for 4 hours. Upon completion of reaction, the product was allowed to cool to room temperature. The product was subsequently collected and washed with ethanol and deionized water for several times to eliminate any unreacted residue. Lastly, the product was dried overnight in a vacuum oven at 60°C, and CN-B in the form of yellow precipitate was obtained.

S2 Nitrogen absorption-desorption isotherm and BJH pore size distribution of CN$_x$-550
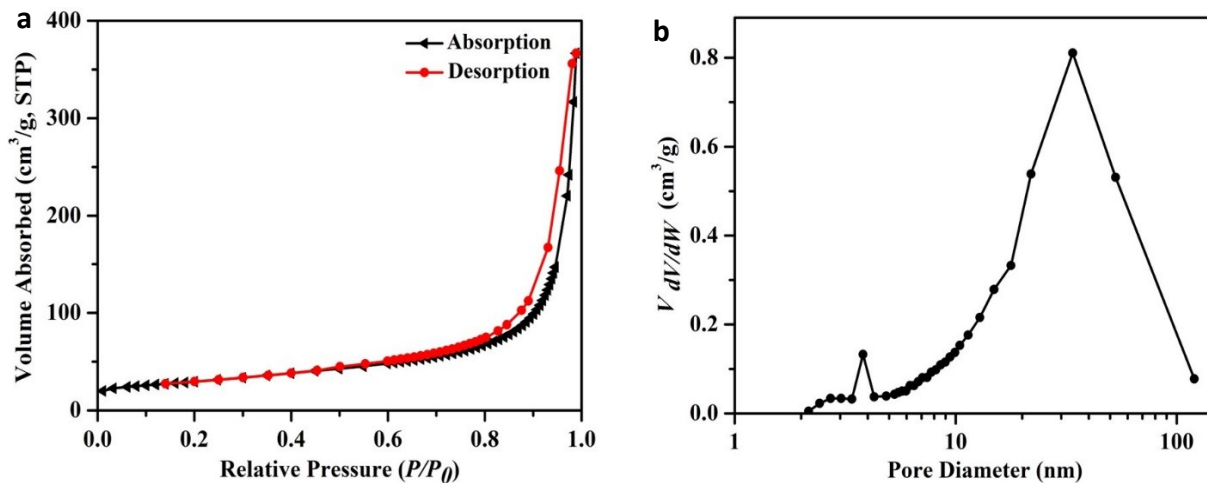
Fig. S1 (a) Nitrogen adsorption-desorption isotherm and (b) BJH pore size distribution of CN$_x$-550.

S3   AFM topographic image of CN-B
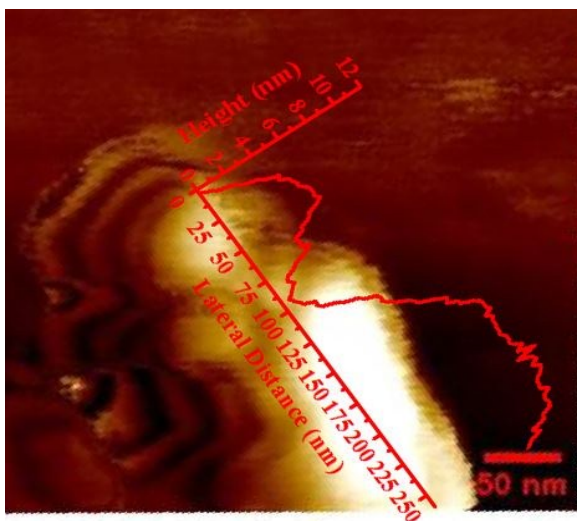
Fig. S2   AFM topographic image and height profile of CN-B.

S4 FTIR characterization

FTIR spectra in Fig. S3 depicts the molecular fingerprints of CN-U and CN_x. The spectra exhibited three characteristic absorption bands of a conventional $g-C_3N_4$ nanomaterials, which are affiliated to: (i) 800 cm^{-1} for stretching of tri-s-triazine units; (ii) 1200 – 1700 cm^{-1} for stretching of C-N heterocycles; and (iii) 3000 – 3400 cm^{-1} for stretching of N-H or O-H functional group. Since the absorption band for N-H and O-H stretching vibrations was overlapped, this posed a challenge in justifying the variation of NH/NH$_2$ species that was involved in the reduction process.[1] The elimination of NH/NH$_2$ species in CN_x could be further evaluated through XPS characterization.
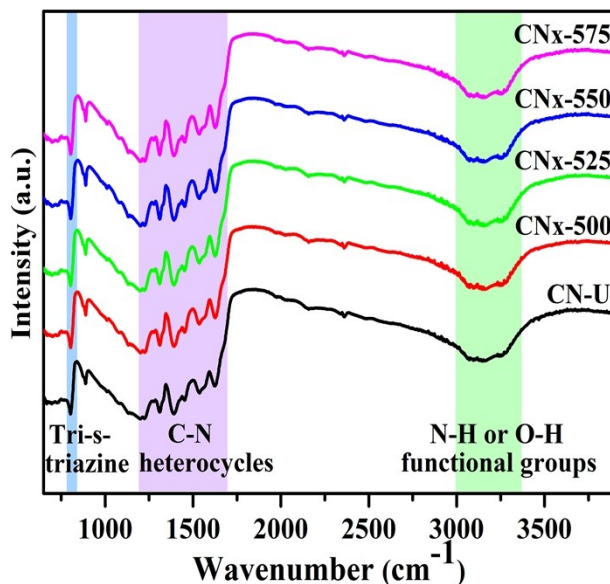
Fig. S3 FTIR spectra of CN-U and CN$_x$.

S5   XPS characaterization of CN$_x$-550
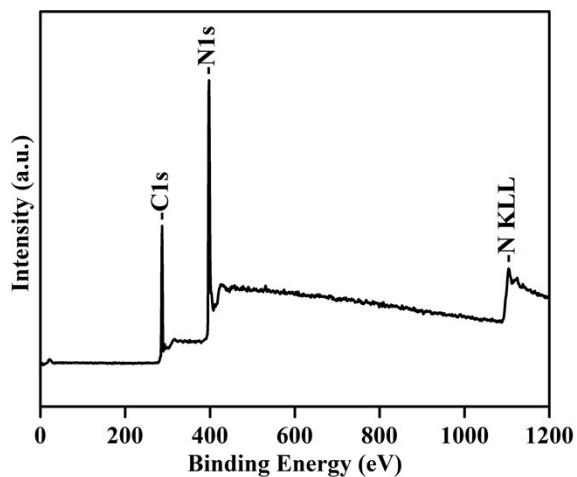
Fig. S4   Full survey XPS spectrum of CN$_x$-550.

Table S1   Elemental composition of CN-U and CN$_x$.

Sample	C at%	N at%	C:N Ratio
CN-U	40.33	59.67	0.676
CN$_x$-500	40.95	59.05	0.693
CN$_x$-525	42.04	57.96	0.725
CN$_x$-550	42.57	57.43	0.741
CN$_x$-575	43.54	56.46	0.771

Table S2   XPS analysis of CN-U and CN$_x$-550.

Sample	C 1s			N 1s		
	Position	Chem. State	At%	Position	Chem. State	At%
CN-U	284.73	C-C	4.73	398.6	N(sp^2)	68.62
	286.11	C-NH$_x$	1.41	399.76	N(sp^3)	22.60
	288.19	N-C-N	93.86	401.03	NH$_x$	8.77
CN$_x$-550	284.88	C-C	1.67	398.6	N(sp^2)	68.42
	285.92	C-NH$_x$	0.41	399.86	N(sp^3)	25.82
	288.29	N-C-N	97.91	401.13	NH$_x$	5.75

S6 UV-Vis characterization
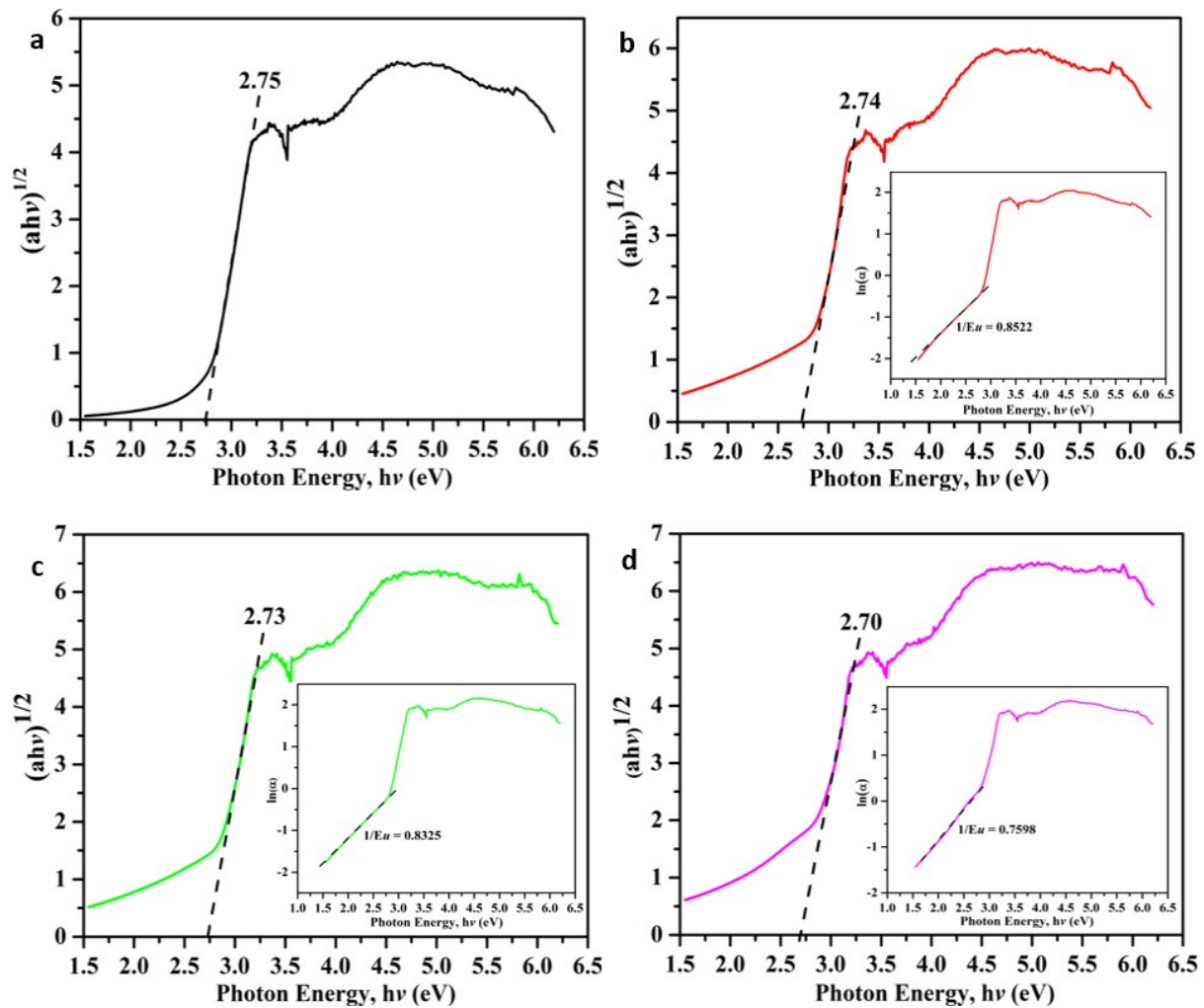
Fig. S5 Tauc plot of transformed KM function versus photon energy of (a) CN-U, (b) CN_x-500, (c) CN_x-525 and (d) CN_x-575. The insets show the corresponding Urbach plot of the sample photocatalysts.

S7   Electrochemical characterization
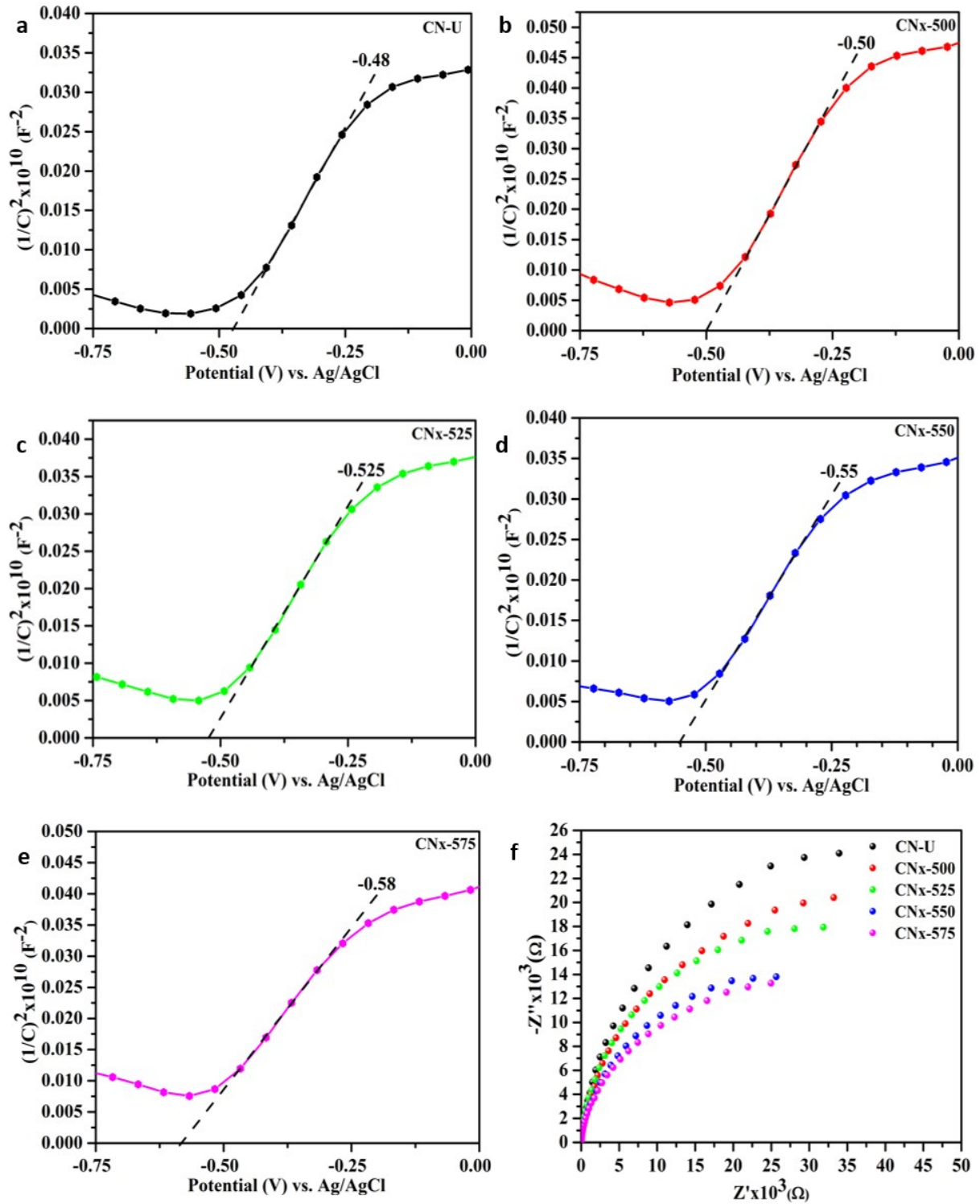
Fig. S6   Electrochemical characterizations of sample photocatalysts. (a-e) Mott-Schottky plot of CN-U, CN_x-500, CN_x-525, CN_x-550 and CN_x-575 respectively. (f) Nyquist plot of CN-U and CN_x.

S8   O$_2$ evolution from photocatalytic CO$_2$ reduction and control experiments

As photocatalytic conversion of CO$_2$ to CH$_4$ gas is a cascade system which involves the oxidation of H$_2$O species and CO$_2$ reduction, thereby a significant amount of O$_2$ gas was detected during the process. The photoreactor was purged thoroughly with humidified CO$_2$ gas prior to photocatalytic reaction for the removal of excess air in the reactor. Nevertheless, O$_2$ and N$_2$ residues remained traceable in the reactor effluent gas. Volumetric ratio of O$_2$ to N$_2$ in the effluent gas was thus measured for better quantification of O$_2$ evolution. As depicted in Fig. S7, a sharp decline in O$_2$:N$_2$ ratio was observed in the first 1 hour of reaction. This drastic change can be ascribed to the consumption of residual O$_2$ to form O$_2^-$ species, as explained in the following equation:[2,3]

$$O_2 + e^- \rightarrow O_2^-$$
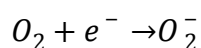
Meanwhile, generation of CH$_4$ from CO$_2$ reduction occurred concurrently upon photoirradiation. The residual O$_2$ competes with CO$_2$ for photogenerated electrons, conducing to less O$_2$ and CH$_4$ products formed. Since the reactor was much concentrated with CO$_2$ gas, there exists a greater tendency for CO$_2$ conversion into CH$_4$ by accepting the photogenerated electrons; while O$_2$ was generated through H$_2$O oxidation with photogenerated holes. O$_2$ evolution eventually outcompetes the consumption of O$_2$ gas, and O$_2$:N$_2$ ratio progressively increased as the reaction proceeded.
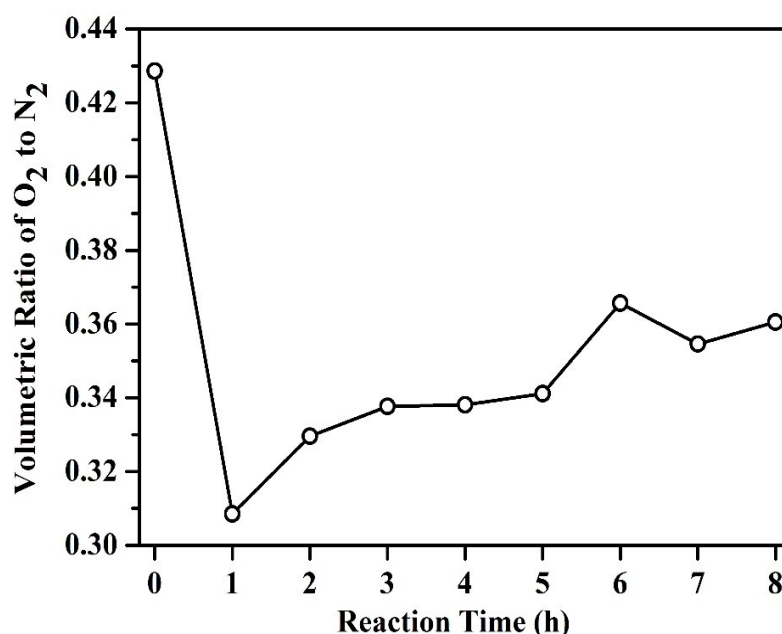
Fig. S7 Time dependence of O$_2$:N$_2$ volumetric ratio during photocatalytic CO$_2$ reduction experiment over CN$_x$-550 under visible light irradiation.
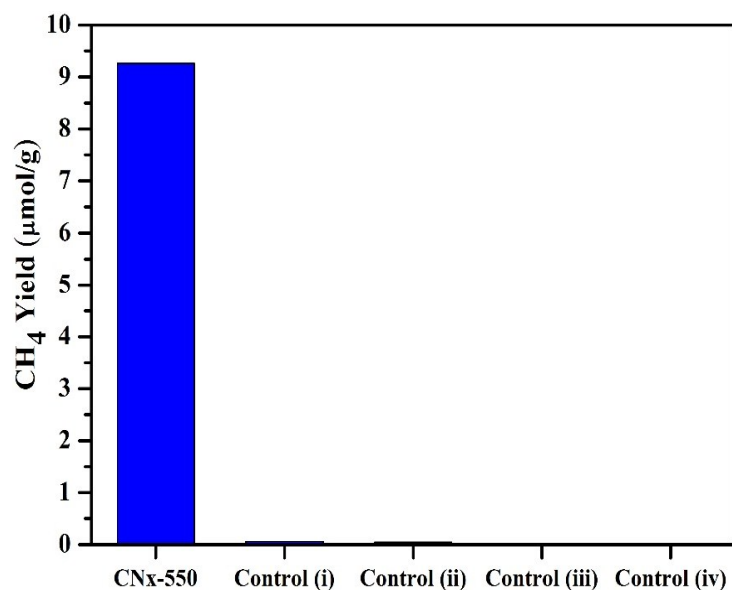
Fig. S8 Yield of photocatalytic CH_4 evolution over CN_x-550 under visible light illumination. Control experiments were performed under four scenarios: (i) under CO_2 flow in the absence of H_2O vapour, (ii) under N_2/H_2O vapour flow, (iii) under CO_2/H_2O vapour environment without photocatalysts and lastly, (iv) in dark condition.

References

1   Z. Hong, B. Shen, Y. Chen, B. Lin and B. Gao, *J. Mater. Chem. A*, 2013, **1**, 11754.

2   X. Y. Kong, W. L. Tan, B.-J. Ng, S.-P. Chai and A. R. Mohamed, *Nano Res.*, 2017, **10**, 1720–1731.

3   H. Zhao, L. Liu, J. M. Andino and Y. Li, *J. Mater. Chem. A*, 2013, **1**, 8209–8216.